Chaos, Solitons & Fractals 45 (2012) 527–538

Contents lists available at SciVerse ScienceDirect

Chaos, Solitons & Fractals

Nonlinear Science, and Nonequilibrium and Complex Phenomena

journal homepage: www.elsevier.com/locate/chaos

Possibilities of introducing different functional circuits on top of a structural neuron triplet: Where do the gains lie?

Igor Franović, Vladimir Miljković *

Faculty of Physics, University of Belgrade, P.O. Box 44, 11001 Belgrade, Serbia

ARTICLE INFO

Article history:
Received 29 April 2011
Accepted 20 August 2011
Available online 28 February 2012

ABSTRACT

Instigated by the research on clusterization phenomena in complex neural networks, we study a triplet of bursting Rulkov map neurons connected via inhibitory synapses with delay. It is demonstrated how on a background of structural motif one can build different types of functional circuits. The approach is based on utilizing the properties of the chemical synapses, whose gating is modeled by the fast threshold modulation, in conjunction with the phase plane analysis, allowing the system state to be represented in terms of maps the neurons reside on. For both the dynamical configurations, monitoring the layout of active neurons, and the functional motifs, following the maps where the synchronized neurons lie, we establish a one-on-one correspondence between sequences in the time series and the triads, making up the subgraphs of the original graph. By introducing the appropriate sets of quantities, one obtains not only the distributions of triads as a function of synaptic parameters, but is also able to identify a distinct triad whose presence may be viewed as a signature of the burst synchronization process. In another setup, the regularization of burst cycles for an arbitrary neuron is explained by classifying all the bursts as long or short, with their fractions linked to the abundances of triads under variation of synaptic parameters.

1. Introduction

One of the most vibrant directions in the research of neural networks unfolds within the realm of complexity, appreciating how both their structural and functional architecture exhibit the features of complex networks [1–5]. What is innate to neuron systems is that their anatomical substrate supports a wide array of coordinated behaviors, but the question as to the exact nature of their relationship remains an elusive one [5–7]. The current evidence suggests how the patterns of functional connectivity at small time scales undergo large fluctuations, being quite responsive to perturbations, whereas for sufficiently long time samples they display formidable robustness, in many cases converging toward their structural counterparts [1,8]. However, there is another less exposed side of the issue, brought up by the fact that the neuron coordination may be expressed in multiple ways. Depending on the focus of the study, one can have diverse functional networks on top of a structural one, though it is less straightforward to predict as to what could be the palpable gains obtained by such an approach. Thus it is our intention not only to reflect on what may be the link between the structural and functional networks, but rather to examine how the comparison between the different types of functional networks may aid in an attempt to reconstruct the a priori unknown structural network.

The graph theoretical tools to describe the structural and functional networks are essentially one and the same. A property that stands out is clusterization, underpinned by the notion of transitivity [7], which is a concept stating that the neurons subjected to the same source are likely to be interconnected as well, or to exhibit the similar behavior. Recalling that the complex networks are

* Corresponding author.
E-mail addresses: igor.franovic@gmail.com (I. Franović), vladimir.miljkovic@ff.bg.ac.rs (V. Miljković).

0960-0779/$ - see front matter © 2012 Elsevier Ltd. All rights reserved.
doi:10.1016/j.chaos.2011.08.013

assembled of small redundant elementary blocks, network motifs [9–11], it is easy to realize how clusterization puts emphasis on the triplets of nodes [6,12–14]. This makes it justified to consider the case of the symmetrical ternary structural motif [6,14] and the effective configurations emerging dynamically by the action of its neurons, where each configuration may be associated with the subgraph of the original graph.

The framework above is best suited for the pulse-coupled networks, a broad [15,16] and well studied subclass [17–21] that has the nodes evolve independently unless the potentials of their neighbors reach a predefined threshold. Such a setup is preferred as it enables one to relate the effective configurations with the states of synaptic openness. Consistent with the findings in several specific brain areas [22,23], we are concerned with a circuit of bursting neurons, here represented by the set of chaotic Rulkov maps [24,25]. Though it may appear crude, the model actually provides a subtle transition between the analysis in the phase plane and the dynamically determined network topology [26,27]. The goal is to highlight the different aspects of the collective phenomena by defining two types of functional networks, one that is based on the number and the layout of active neurons, whereas the other takes into account whether there is burst synchronization as well as the set of maps occupied by the neurons. Adopting either classification, we were able to establish a one-on-one correspondence between the sequences within the time series and the effective circuits, dubbed dynamical configurations and the functional motifs, respectively.

The paper is organized as follows. After an overview of the phase plane analysis, the Section 2 deals with the formal definitions regarding the dynamical configurations and functional motifs by assigning them the appropriate triad classes and introducing the quantities to characterize their presence within the time series. In the Section 3 it is demonstrated how the variation of synaptic parameters has some triads more populated, whereas the others are left vacant, also discussing how the approaches laid out may work as complementary when determining the triad roles with respect to synchronization. Additional arguments are drawn from examining how the interaction reflects in the regularization of the neuron's bursting series. The concluding remarks are provided to summarize the results obtained and to outline the directions for future study.

2. Model and the applied methods

To describe the dynamics of the coupled neuron i one adopts a two-dimensional map of the form

$$x_{i,n+1} = \frac{\alpha}{1+x_{i,n}^2} + y_{i,n} - \sum_{i\neq j} g_{c,ij}(x_{i,n}-v)\frac{1}{1+\exp(-k(x_{j,n-\tau}-\theta))},$$
$$y_{i,n+1} = y_{i,n} - \mu(x_{i,n}-\sigma), \qquad (1)$$

where the sum runs over the presynaptic neurons, and n denotes the iteration step. Without the interaction term, Eq. (1) amounts to the chaotic Rulkov model that generates square-wave bursts [24] under the appropriate set of parameters. Letting $\mu = 0.001$, there is a sharp separation of time scales between the respective fast and slow variables $x_{i,n}$ and $y_{i,n}$, such that the former may embody the membrane potential, and the action of the latter is reminiscent of that of the gating variables. As expected from the phenomenological model, some of the variables, most notably α, make no reference to any physiological processes. If compelled to choose between the conductance-based models, it can be argued for that of Hindmarsh–Rose to present the closest counterpart to the Rulkov map, both in terms of the phase space structure [25,28] and the exhibited dynamical modes [29,30]. Regarding the isolated neuron, a brief survey of the analysis treating $y_{i,n}$ as a control parameter γ within the fast subsystem is appended with Fig. 1, whereas a comprehensive review may be found in [25,29]. In a nutshell, the motion of the phase point is guided by the fast nullclines, joined in an S-curve, and the curves of minimal and maximal map iterates, Ξ_{min} and Ξ_{max}, that provide for the burst envelopes. What is essential here is how the bursting dynamics relies on the existence of the bistability region in the fast subsystem, arising if $\alpha > 4$. Varying α can also be used to control the irregularity of bursts: the closer α gets to 4, the less chaotic the bursting series becomes. Throughout the paper we select $\alpha = 4.15$ that warrants a reasonable tradeoff between the duration of bursts and the stochastic effects involved in their termination [22,25]. Nonetheless, adjusting α to other values may evoke different forms of neuronal dynamics, including excitable behavior ($\alpha < 2$), periodic pulses or bursts ($2 < \alpha < 4$), as well as chaotic pulses for $\alpha > 4.6$ [31]. To conclude with the autonomous neuron parameters, the external dc bias current σ is taken to be uniform, assuming the value $\sigma = -0.9$.

To set up the desired symmetrical ternary circuit, cf. Fig. 2(a), one needs to take care of several details within the interaction term. First, the synaptic weights have all been assigned an equal value, $g_{c,ij} = g_c$, abandoning this only late in the paper, when we discuss how the inhomogeneity reflects on the results obtained. The synapses are made inhibitory by virtue of the reversal potential $v = -1.8$ [22]. The gating behavior is represented by a sigmoid function, where the sharpness of the response depends on the gain parameter k [17,30,32]. The value $k = 25$ selected here is consistent with the fast threshold modulation model (FTM) [33], known to approximate well the action of the majority of chemical synapses in the brain [34,35]. For simplicity, the activation thresholds are held homogeneous, ensuring that $\theta = -1.4$ is easily reached by a bursting neuron. Finally, the time lag τ is incorporated such that the gate opening is influenced by the delayed arrival of the presynaptic potentials. By variation of the delay alone, one can achieve different forms of neuron coordination, as illustrated in Fig. 2(b) and (c).

Proceeding to the main topic of our paper, we first discuss the steps required to raise the description of system evolution from the level of collection of individual neuron states onto that of succession between the effective network configurations. To this end, it is convenient to convert time series of membrane potentials into binary symbolic sequences $\Phi(i,n)$. The coding transformation T is such that it ascribes $\Phi(i,n) = 1$ if a neuron is bursting, and 0 otherwise:

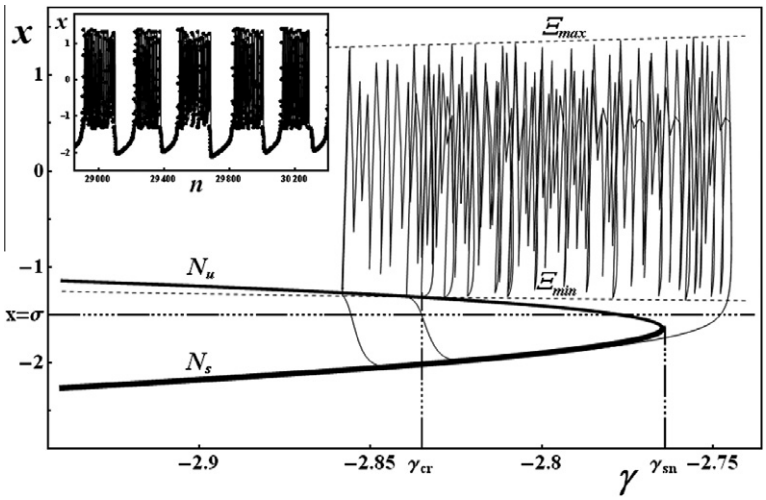

Fig. 1. Enlarged bistability region of the fast subsystem. The map admits bursting if there is an intersection between the slow variable nullcline $x_n = \sigma$ and the branch of unstable fixed points N_u, such that γ increases (decreases) whenever the phase point lies below (above) the slow nullcline. The saddle-node bifurcation $\gamma = \gamma_{sn}$ and the external crisis $\gamma = \gamma_{cr}$ mark the approximate boundaries of a burst, whereas ascending the stable branch N_s coincides with the interburst intervals. The irregularity in the series of an autonomous neuron derives from the burst termination that occurs at random when the phase point has passed γ_{cr}. The inset displays a typical waveform obtained for $\alpha = 4.15$ and $\sigma = -0.9$.

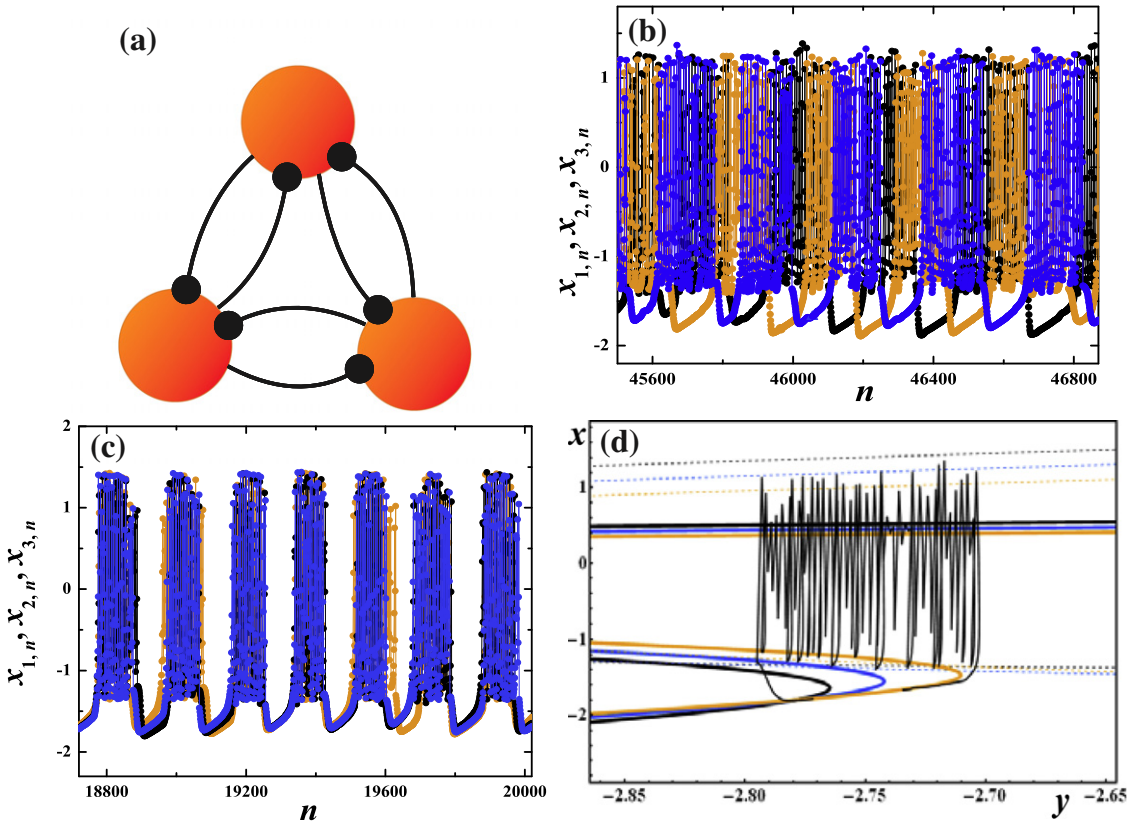

Fig. 2. (a) Schematic display of the symmetrical ternary structural motif, where nodes depict the neurons, and the dots represent the synapses. In (b) and (c) the focus is on the impact of time delay on the fast variables' waveforms coded black, blue (dark grey) and orange (light grey), keeping the fixed weight $g_c = 0.11$. Obtained for the small delay $\tau = 10$, (b) shows sequences of partial burst synchronization that involve pairs of neurons cyclically switching between the episodes. The large delay $\tau = 90$ in (c) is seen to give rise to approximate synchronization in-phase with all the three neurons taking part. (d) A burst orbit from (b) is extracted into the phase plane, whose layout is determined by the three relevant maps, including the isolated one (black solid and dashed lines) and the two interacting maps, g_c and $2g_c$, presented by blue (dark grey) and orange (light grey), respectively. For interpretation of the references to colour in this figure legend, the reader is referred to the web version of this article.

$$\Phi(i,n) = T(x_{i,n}) = \begin{cases} 1, & x_{i,n} \text{ in the bursting range;} \\ 0, & x_{i,n} \text{ in the silence range,} \end{cases} \quad (2)$$

where the discretization is performed by a useful rule of thumb relating bursting (silence) to potentials lying above (below) θ. A substantial gain from the model applied presents an easy blending between a more straightforward setup putting emphasis on the bursting activity, or rather the states of synaptic openness, and the alternative map approach, that derives from the phase plane analysis. To recap on the latter, we have previously shown how with the inclusion of interaction the original neuron map gets shifted rightward and upward in the phase plane, but carries over the shape and the stability features of the curves of fixed points [26,27,29]. This is what allows one to represent the neuron dynamics in terms of switches between the isolated and the relevant interaction maps, which only holds exactly due to synaptic states being either open or closed, a corollary of the FTM. For the symmetrical triplet, the interacting maps involved are g_c and $2g_c$, see Fig. 2(d).

Focusing on different collective phenomena, during the course of time changes of the neuron states get reflected in reconfiguration of the effective network topology. At least in principle, there is nothing to prevent us from defining multiple types of functional circuits on top of the same structural one. Thus, unlike the analysis for the neuron couple [27], here it turns out useful to distinguish between the "barren" system dynamics and the dynamics along the path to synchronization, embodied by the two sets of effective circuits we dub dynamical configurations and functional motifs, respectively. Either way, one resorts to classification by assigning their members the subgraphs of the original three node graph, which comes down to an issue resolved in the Alon's "motif dictionary" [5,6,36], where by counting in both the connected and the unconnected subgraphs it is arrived to a total of 16 distinct triads, cf. Fig. 3.

The notion of dynamical configuration refers to the state of openness of all the synapses contained in the structural motif. By letting the synapses be homogeneous, admissible are only the triads whose nodes have all the outward synapses either open or closed at the time. This effectively reduces their number from 16 to 4, that one may designate according to the number of active neurons, N_1, and those inactive, N_0, enforcing the natural interpretation in terms of the motif's "occupation numbers". Extending the similar kind of reasoning to an arbitrary N-size homogeneous system of all-to-all pulse-coupled neurons, we provide a template for representing its dynamics solely via the evolution of an effective network. This is carried out by introducing the quantities

$$c_{N_1,N_0} = \left\langle \left\langle \frac{N_1!N_0!}{N!} \sum_{p\in\{0,1\}} \widehat{P} \prod_{i}^{N_1} \delta_{\Phi(i,n),1} \prod_{i=N_1+1}^{N} \delta_{\Phi(i,n),0} \right\rangle \right\rangle, \quad (3)$$

that characterize the contribution from each dynamical configuration determined by the occupation numbers. From now on, δ is reserved for the Kronecker's delta symbol, products of which make up a suitable formalism to write down the desired configuration of active neurons, as extracted from the set of all possible states. In Eq. (3), brackets $\langle\langle \ldots \rangle\rangle$ signify double averaging, temporal and over a set of different initial conditions. Given the network invariance under permutation of nodes, the symmetrizing operator $\frac{1}{N!}\sum_{p\in\{0,1\}} \widehat{P}$ is necessary to account for the degeneracy of each configuration.

Applying the definition above to the 4 possible triads of the symmetrical triplet, one arrives at the expressions in which the action of the symmetrizing operator is made explicit

$$\begin{aligned} c_{03}^{(14)} &= \langle\langle \delta_{\Phi(1,n),0}\delta_{\Phi(2,n),0}\delta_{\Phi(3,n),0}\rangle\rangle, \\ c_{12}^{(1)} &= \frac{1}{3}\langle\langle \delta_{\Phi(1,n),0}\delta_{\Phi(2,n),0}\delta_{\Phi(3,n),1} + \delta_{\Phi(1,n),0}\delta_{\Phi(2,n),1}\delta_{\Phi(3,n),0} \\ &\quad + \delta_{\Phi(1,n),1}\delta_{\Phi(2,n),0}\delta_{\Phi(3,n),0}\rangle\rangle, \\ c_{21}^{(6)} &= \frac{1}{3}\langle\langle \delta_{\Phi(1,n),0}\delta_{\Phi(2,n),1}\delta_{\Phi(3,n),1} + \delta_{\Phi(1,n),1}\delta_{\Phi(2,n),0}\delta_{\Phi(3,n),1} \\ &\quad + \delta_{\Phi(1,n),1}\delta_{\Phi(2,n),1}\delta_{\Phi(3,n),0}\rangle\rangle, \\ c_{30}^{(13)} &= \langle\langle \delta_{\Phi(1,n),1}\delta_{\Phi(2,n),1}\delta_{\Phi(3,n),1}\rangle\rangle. \end{aligned} \quad (4)$$

Here, by the order of display, the lower indices refer to configurations with no, one, two or three neurons bursting. The superscripts coincide with the triad IDs from Fig. 3.

In order to characterize the functional motifs we introduce the quantities that take into account how well are matched the intervals of bursting or silence between all three neurons. When synchronized, each of the neurons may lie on either the isolated, g_c or $2g_c$ map, which makes

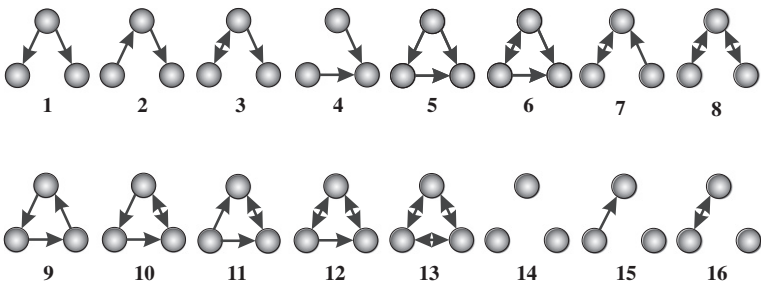

Fig. 3. Classification of all possible graphs with three nodes and directed edges, where both the connected (first 13 items) and the unconnected triads (last 3 items) are counted in. Each and every effective circuit arising from the initial structural motif can be cast as a member of one of the classes enumerated. Depending on the model details, some classes may as well prove absent altogether, viz. here the assumed homogeneity of synaptic thresholds rules out all but the triads 1, 6, 13 and 14, dubbed single-tail (*ST*), double-tail (*DT*), totally connected (*TC*) and totally unconnected (*TU*), respectively.

it convenient to label their corresponding states with 0,1 and 2 for shorthand. The particular set of maps occupied is the key for discriminating between the functional motifs. Their contributions in the synchronization process are described by the quantities

$$h_{ijk} = \left\langle\left\langle \delta_{\Phi(1,n),\Phi(2,n)}\delta_{\Phi(2,n),\Phi(3,n)} \frac{(i+j+k2)!\left(3-\frac{i+j+k}{2}\right)!}{3!} \times \sum_{p\in\{0,1\}} \widehat{P}\prod_{l}^{\frac{i+j+k}{2}} \delta_{\Phi(l,n-\tau),1} \prod_{l=\frac{i+j+k}{2}+1}^{3} \delta_{\Phi(l,n-\tau),0} \right\rangle\right\rangle, \quad (5)$$

where $i, j, k \in \{0,1,2\}$ refer to the state of each neuron, and the presence of τ reflects the point of such states being determined by the delayed arrival of the presynaptic potentials. Adhering to the notation from the Eq. (3), here we only remark how $\frac{i+j+k}{2}$ equals the number of bursting neurons, implying the existence of 4 admissible functional motifs that are again associated with the triads 1, 6, 13 and 14 from Fig. 3. One readily acquires the appropriate h-quantities

$$\begin{aligned}
h_{000}^{(14)} &= \langle\langle \delta_{\Phi(1,n),\Phi(2,n)}\delta_{\Phi(2,n),\Phi(3,n)}\delta_{\Phi(1,n-\tau),0}\delta_{\Phi(2,n-\tau),0}\delta_{\Phi(3,n-\tau),0}\rangle\rangle,\\
h_{011}^{(1)} &= \frac{1}{3}\langle\langle \delta_{\Phi(1,n),\Phi(2,n)}\delta_{\Phi(2,n),\Phi(3,n)}(\delta_{\Phi(1,n-\tau),1}\delta_{\Phi(2,n-\tau),0}\delta_{\Phi(3,n-\tau),0}\\
&\quad + \delta_{\Phi(1,n-\tau),0}\delta_{\Phi(2,n-\tau),1}\delta_{\Phi(3,n-\tau),0}\\
&\quad + \delta_{\Phi(1,n-\tau),0}\delta_{\Phi(2,n-\tau),0}\delta_{\Phi(3,n-\tau),1})\rangle\rangle,\\
h_{112}^{(6)} &= \frac{1}{3}\langle\langle \delta_{\Phi(1,n),\Phi(2,n)}\delta_{\Phi(2,n),\Phi(3,n)}(\delta_{\Phi(1,n-\tau),1}\delta_{\Phi(2,n-\tau),1}\delta_{\Phi(3,n-\tau),0}\\
&\quad + \delta_{\Phi(1,n-\tau),0}\delta_{\Phi(2,n-\tau),1}\delta_{\Phi(3,n-\tau),1}\\
&\quad + \delta_{\Phi(1,n-\tau),1}\delta_{\Phi(2,n-\tau),0}\delta_{\Phi(3,n-\tau),1})\rangle\rangle,\\
h_{222}^{(13)} &= \langle\langle \delta_{\Phi(1,n),\Phi(2,n)}\delta_{\Phi(2,n),\Phi(3,n)}\delta_{\Phi(1,n-\tau),1}\delta_{\Phi(2,n-\tau),1}\delta_{\Phi(3,n-\tau),1}\rangle\rangle,
\end{aligned} \quad (6)$$

providing the fractions of distinct functional motifs within the time series for each selection of (g_c, τ). Notably, unlike the c-quantities whose sum equals 1 for arbitrary (g_c, τ), the sum of h-quantities is always less than 1. In the remainder, we also consider why the c- and h-quantities, assigned to particular triads, depart from or approach each other when changing the synaptic parameters. For easy recognition, instead of applying the numerical IDs, the triads 1, 6, 13 and 14 are addressed by the codenames single tail (*ST*, where the term tail refers to a transmitter node), double tail (*DT*), totally connected (*TC*) and totally unconnected (*TU*), respectively. To obtain the results below, we performed time averaging over the long series of 50,000 iteration steps and a set of a 1000 different initial conditions.

3. Results

To get a sense of the general tendencies in the activity of the circuit, we first inspect the field of quantity H under variation of g_c and τ, see Fig. 4. Given that each point in this plane may be associated with a specific type of waveforms, the shading pattern suggests how for a limited range of weights enhancing the delay eventually leads to an approximate synchronization in phase. Examining as to why there is such an upper boundary on g_c, unreported previously in the two-neuron case [26,27], one realizes

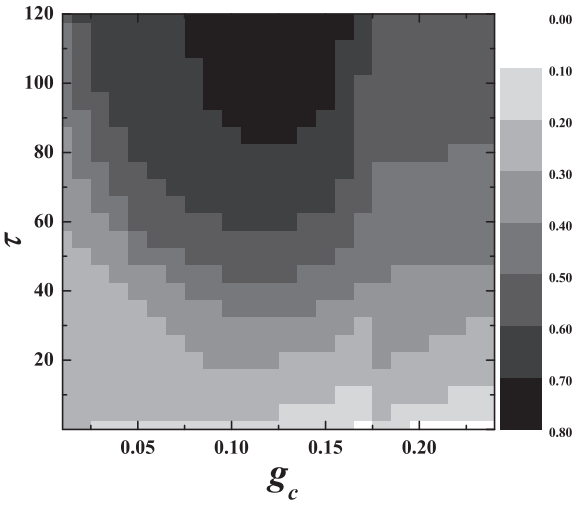

Fig. 4. Quantity H field in the (g_c, τ) parameter plane. The darker shading reflects how enhancing delay gives rise to burst synchronization. Displayed darkest is the domain of maximal synchronization (DMS), where the approximate synchronization in-phase between all three neurons sets in. The features of the $2g_c$ map for $g_c \gtrsim 0.17$ see the profiles of the shaded regions to flatten out, as the system's behavior becomes virtually independent on weight.

that it derives from the very properties of the interacting Rulkov map and is related to the collapse of the external crisis for $2g_c$ above 0.34, where the intersection between the curves of minimum iterates and the branch of unstable fixed points is lost. For the moment we refrain from entering deeper into the analysis of the path to synchronization, but instead touch upon the phenomena exhibited for the delays close to its endpoints by taking another look at the time series in Fig. 2(b) and (c). Selecting the small τ, one frequently encounters pairs of active neurons engaged in a partial burst synchronization, whereas with each episode the different neuron is left silent. Once τ is sufficiently increased, the approximate synchronization in phase that sets in will be better or worse depending on the interplay with g_c. In this context, the existence of the domain of maximal synchronization (DMS) should be singled out, as it warrants the least deviations from the preferred regime, cf. the parameter region displayed darkest in Fig. 4.

To prepare the appropriate setting for the discussion ahead, we now focus on the circuit dynamics devoid of any synchronization properties by considering the role the dynamical configurations, introduced earlier, assume within the time series. As it stands, their presence does not merely witness on the current layout of the open synapses, but also, given the synaptic delay, provides a glimpse at which set of maps the neurons will occupy after the next τ steps. Translated into the language of triads from Fig. 3, by the latter is meant how in case of the *ST* configuration one deduces that the neuron whose outgoing synapses are open will reside on the isolated map, and the two receiving neurons will be on the $1g_c$ maps, with the similar kind of reasoning available in the three remaining instances. As to why the c-quantities for the specific configurations may be relevant is easily explained by observing side-by-side their variation along the two char-

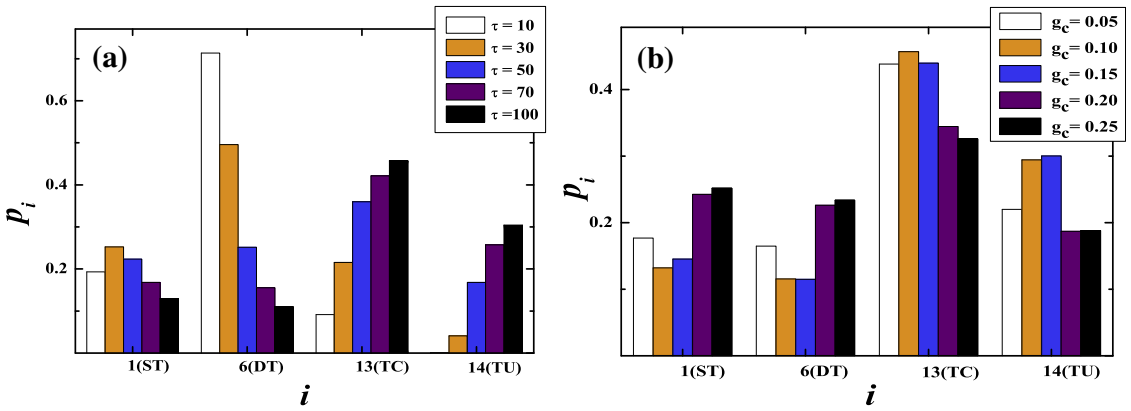

Fig. 5. Side-by-side decomposition of the collective neuron dynamics via the c-terms maintaining fixed $g_c = 0.11$ in (a) and $\tau = 100$ in (b). The contiguous bars refer to fractions of the particular dynamical configurations, indexed numerically and by codenames, under variation of the remaining parameter. Comparison between (a) and (b) yields the prevailing dependence of the c-quantities on the increase of τ and only a minor change with g_c.

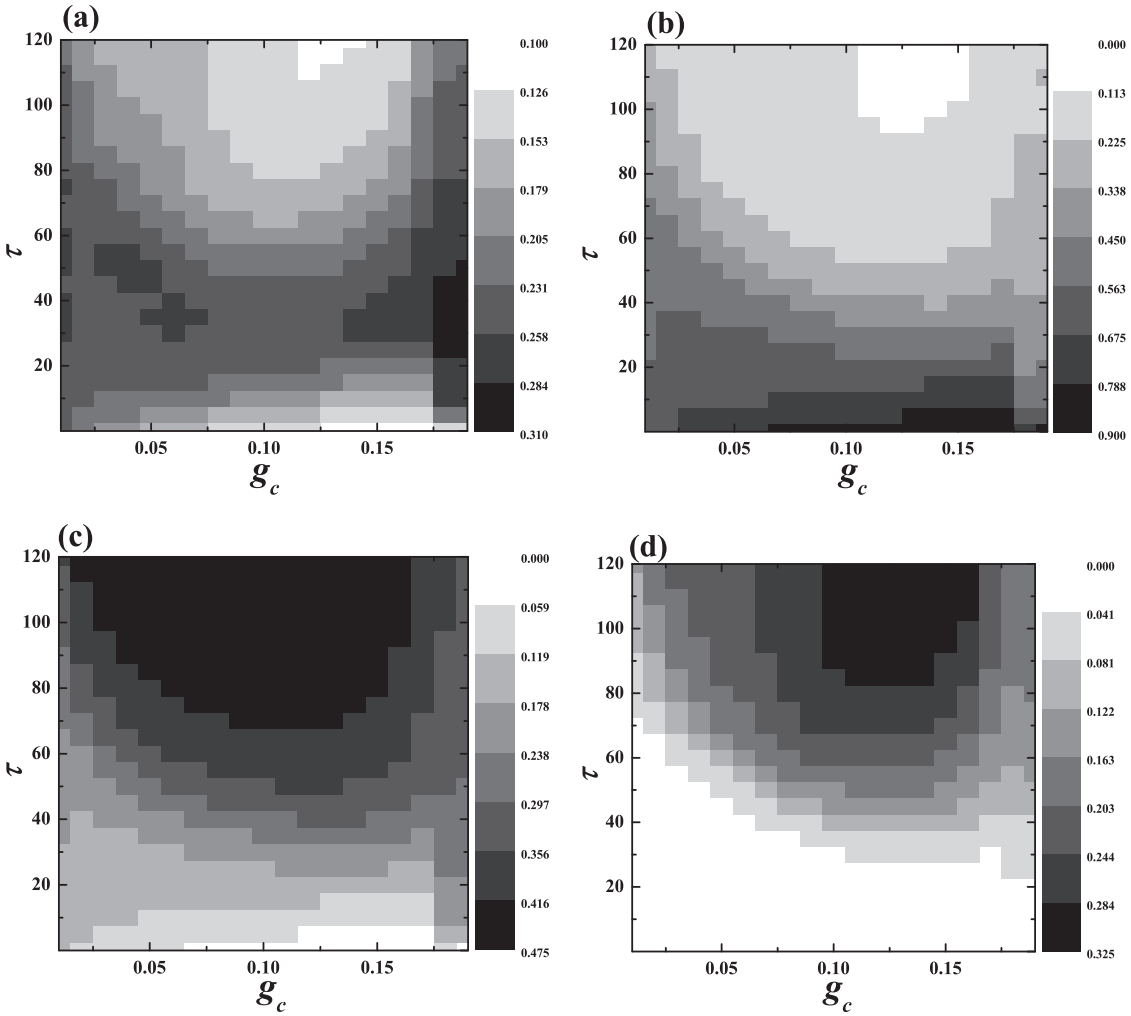

Fig. 6. Fields of c-quantities in dependence of g_c and τ, with the plots in (a), (b), (c) and (d) referring to the *ST*, *DT*, *TC* and *TU* dynamical configurations, respectively. Comparison between the four shows the area of small τ and moderate g_c being the sole instance when the system comes close to a pure state, namely the one coinciding with the *DT* triad. For the larger delays, the bottom row witnesses the increase of *TC* and *TU* terms, countered by the respective declines of the *DT* and *ST* terms in the top row.

acteristic directions in the (g_c,τ)-plane. One of them coincides with the increase of τ at fixed g_c (Fig. 5(a)), while the other is taken mutatis mutandis (Fig. 5(b)), but both are chosen so as to transit the DMS. In either case, the particular configurations can be mapped onto the states of the neuron system, and their c-values may be looked upon as probabilities to find the system in those states. In terms of collective behavior, from Fig. 5(a) we learn about the general tendency for τ to give rise to the *TC* and *TU* fractions, and to cause the decline of the *ST* and *DT* ones. As far as the fixed τ direction is concerned, Fig. 5(b) tells us that g_c affects the occupation of the dynamical configurations only negligibly, so that their respective ratios are largely maintained. Nonetheless, this holds true only for the range delimited by the properties of the interacting map ($g_c \leqslant 0.17$), outside of which the occupations are likely to level each other out.

After providing a more general picture, let us fill in the details by extending the analysis above to fields of c-quantities within the (g_c,τ) parameter plane. In view of Fig. 6(a)–(d), one not only notes how the increase of τ affects the occupations causing migration from the states *ST* and *DT* to *TC* and *TU*, but also finds that c_{TC} rises at the expense of c_{DT}, and c_{TU} on the account of c_{ST}. Another interesting point recovered is that the system can be taken into a virtually "pure" state only for small τ and for sufficiently large g_c, contrary to the common logic expecting a pure state for the weakly interacting system.

Each dynamical configuration can play a dual role, constructive or destructive in respect to synchronization. To gain an insight into the path to synchronization itself one is required to single out the fractions of time the system resides on the particular functional motifs, which is expressed by the appropriate h-quantities. In other words,

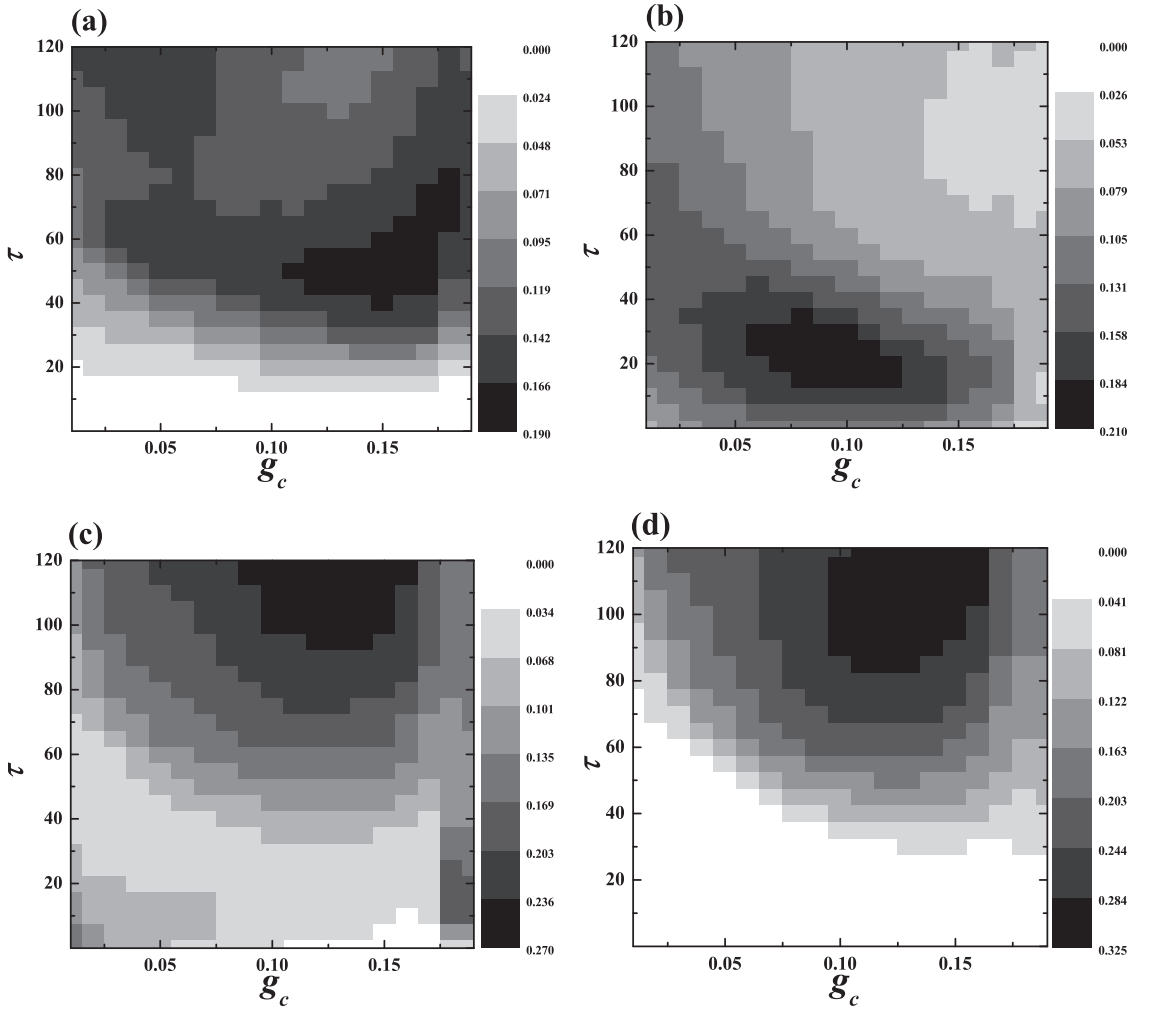

Fig. 7. Fields of h-quantities in the (g_c,τ) parameter plane display the representation of the functional motifs, such that (a) corresponds to the *ST* triad, (b) to the *DT* and (c) to the *TC* triads, whereas (d) is provided for the *TU* triad. From the top row, noteworthy are the "synchronization eye" in the *DT* motif for moderate τ and the highest values of the *ST* term, observed at the intermediate delays. From the bottom row, one reads the increasing contribution of the *TC* triad with τ, and in particular, the rise of the *TU* contribution from virtually nonexistent at small τ to the position of the prevailing factor at large delays. Appreciating its unique role in the synchronization process, the *TU* triad is referred to as "synchronizing".

states pertaining to the functional motifs are extracted from the set of all possible states provided by the dynamical configurations, such that $h_i \leqslant c_i \, \forall \, i \in \{1,6,13,14\}$ always holds. As with the c-quantities, for the h-quantities the dependence on τ again prevails in the (g_c, τ) plane, cf. Fig. 7. For small τ, the marginal overlap of bursts is manifested by the parallel increase of the factors corresponding to the *TC* and *DT* motifs, whereby *DT* wins over at somewhat higher τ, as evident from the "synchronization eye" in the lower section of Fig. 7(b). The first visible step to synchronization presents the occurrence of the h-term corresponding to the *TU* motif, recorded for the intermediary delays, see Fig. 7(d). At this stage, there is also a minor contribution to synchronization by the *ST* motif, whose fraction reduces with τ. Further enhancing the delay, one approaches the genuine phase synchronization, where the neurons burst together following the isolated map, and are silent while on the $2g_c$ map, a scheme reflected by the large values of h_{TU} and h_{TC}.

Making comparison between Figs. 6 and 7, some interesting conclusions can be drawn regarding the *TC* and *TU* motifs. For the latter, the h and c values are exactly identical, which makes it justified to dub the *TU* motif synchronizing. The reason for this in terms of the map dynamics will be explained more closely later on. Nonetheless, the *TC* motif at large τ seems to play a more ambiguous role, for as much as it contributes synchronization during the

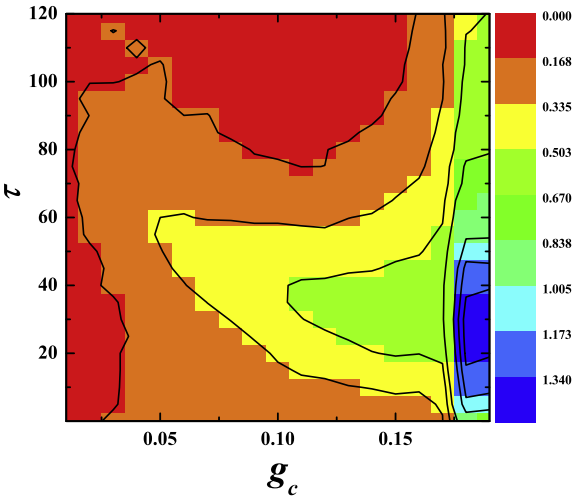

Fig. 9. Contour plot of the regularity field R with respect to g_c and τ, such that smaller values indicate areas with higher periodicity of the bursting cycles. The color bar is set so its blue end points to a lesser periodicity. The results imply almost regular bursting for most of the parameter plane, except for the area of intermediate delays and larger weights, where the "irregularity tongue" is situated. Letting the weights assume values above the limit $g_c = 0.17$, imposed by the features of the interacting Rulkov map, induces further rise in irregularity of the bursting series. For interpretation of the references to colour in this figure legend, the reader is referred to the web version of this article.

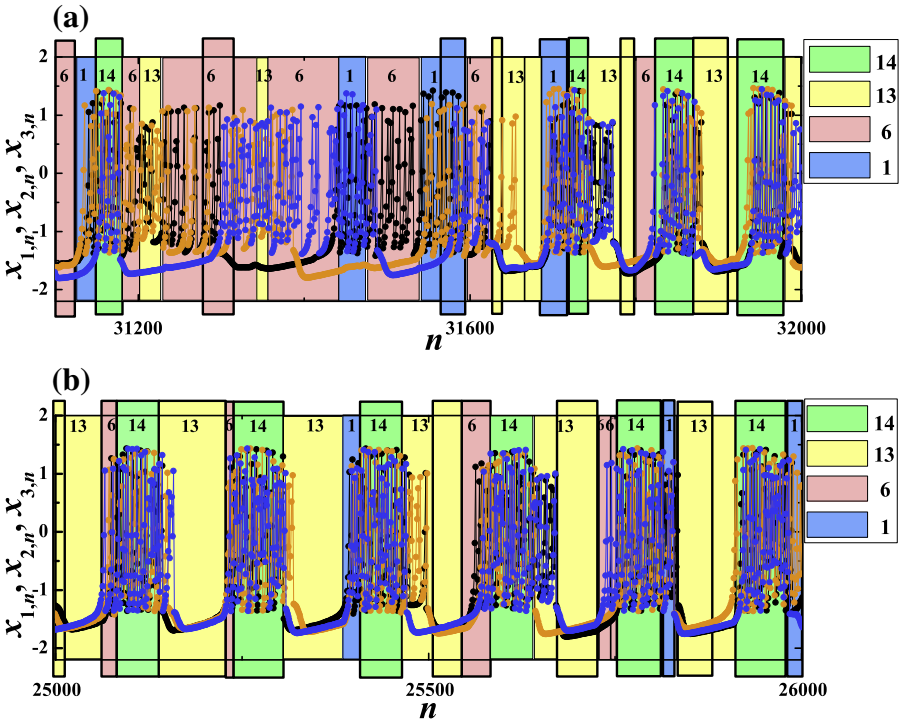

Fig. 8. Dividing the neurons' time series into segments attributed to distinct dynamical configurations and functional motifs made explicit for $\tau = 50$ in (a) and $\tau = 80$ in (b) under equal weight $g_c = 0.11$. In difference to dynamical configurations, the functional motifs are inscribed within the stretched rectangles, applying for the appropriate triads in either case the color-coding (blue, pink, yellow and green stand for *ST*, *DT*, *TC* and *TU*, respectively) as well as the numerical labeling scheme from Fig. 3. In (a), all the dynamical configurations are present, whereas the occurrences of functional motifs are sporadic. For the larger delays, the share of the *TC* and *TU* configurations is overwhelming, and one notes a significant overlap between them and the coincident motifs, arising as a result of the increased burst synchronization. For interpretation of the references to colour in this figure legend, the reader is referred to the web version of this article.

silent intervals, one also frequently finds the setup when two neurons are silent while the remaining bursts on the $2g_c$ map. These and similar claims are witnessed by the displayed in Fig. 8, demonstrating how the time series can be partitioned into sequences that belong to distinct dynamical configurations (normal rectangles) and the functional motifs (stretched rectangles). Evidently, the more the synchronization sets in, the longer are the sections covered by the stretched rectangles. From Fig. 8(a) and (b) we also learn something that cannot be read from the dependence of the h-quantities: as τ rises, the frequency of transitions between different motifs gets increased.

Setting aside the framework laid out by the functional motifs and their relationship with the dynamical configurations, let us explore whether it is possible to extend to larger systems the link between the burst synchronization and regularization, a point previously highlighted for the neuron couple [24,27]. To test for the periodicity within the burst sequences, it is convenient to introduce the regularity quantity [31,37,38]

$$R = \frac{\sqrt{\langle\langle l^2\rangle\rangle - \langle\langle l\rangle\rangle^2}}{\langle\langle l\rangle\rangle}, \tag{7}$$

where l denotes the duration of the burst cycle, viz. time from the one burst's onset to the next, and $\langle\langle\cdot\rangle\rangle$ stand for the averages taken over a long time series and a set of 1000 trials with different initial conditions. Given that R is defined as the normalized fluctuation of the burst cycles, its smaller values signify lesser variability in cycle length, which provides for the higher regularity. The R-field in Fig. 9 shows how the parameter region with the largest periodicity approximately matches that of maximal synchronization from Fig. 4. The other important insight concerns the existence of the tongue-like area of irregularity stretching out to $\tau \approx 60$ iteration steps, with the highest R values seen leaning toward larger g_c.

To address these issues, one first invokes the argument from [26], where we have demonstrated for a neuron couple how it is possible to distinguish between only two types

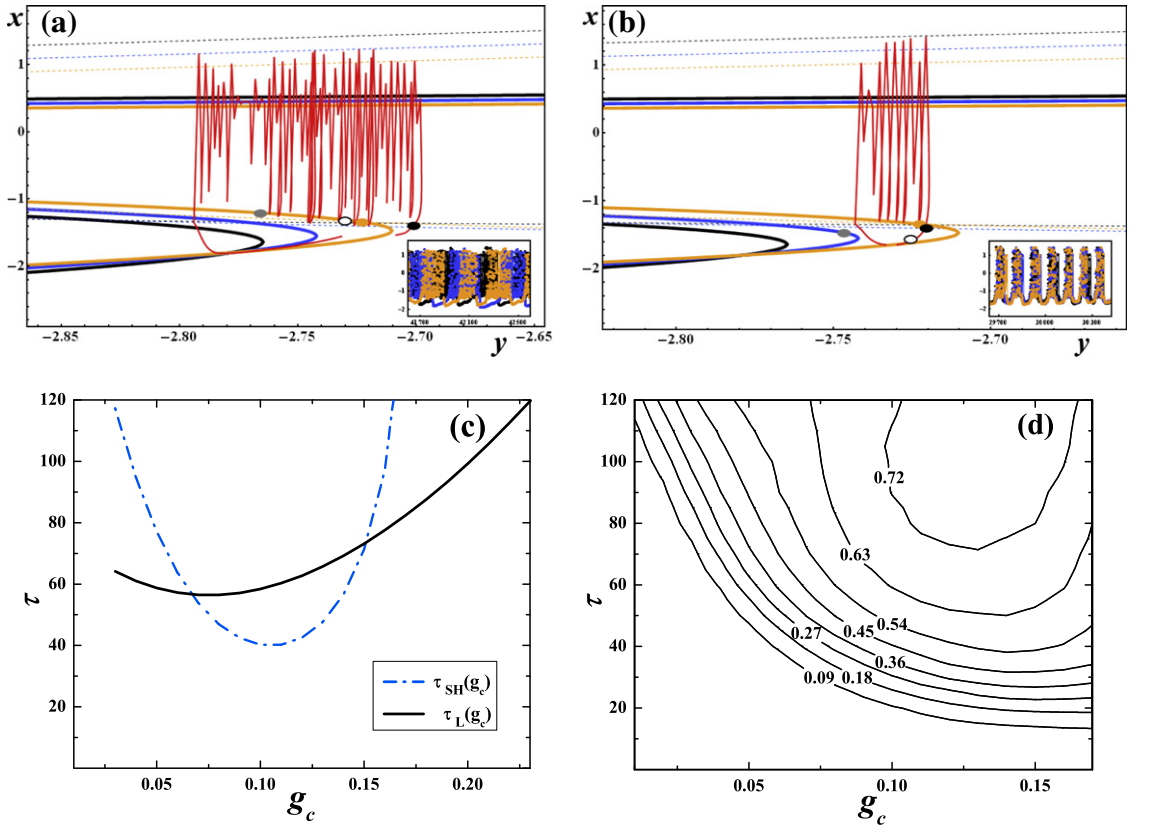

Fig. 10. (a) The main frame displays a typical waveform of a long burst embedded in the phase plane, taking the particular example from a neuron's series for $(g_c, \tau) = (0.11, 65)$. At the moment of triggering the burst (phase point depicted black), the given neuron "sees" the remaining couple with a τ-step delay, when their respective positions were in site of the grey and the empty bullet. The orange (light grey) bullet denotes the external crisis of the $2g_c$ map, whereas the inset shows the sequences of all three neurons overlapped. (b) Waveform of a typical short burst, with the neuron parameters and the notation the same as in (a). As opposed to the arising of long bursts, the onset of short ones is most likely to follow the release mechanism. (c) Assuming the kind of long and short bursts presented in (a) and (b) to be prevailing within the time series, one is able to calculate the curves $\tau_{SH}(g_c)$ and $\tau_L(g_c)$, where the former refers to the first occurrence of the short bursts, and the latter predicts the delay values above which the number of long bursts declines sharply. (d) Contour map for the fraction of short bursts in the neuron series as a function of g_c and τ. The curves represent averages over a 1000 runs with different initial conditions. For interpretation of the references to colour in this figure legend, the reader is referred to the web version of this article.

of bursts, namely the short and the long ones, such that the former are completed in about τ steps. The goal has been to present the path toward phase synchronization in terms of the occurrence and the eventual prevalence of short over the long bursts. The ternary system can be treated in a similar fashion, though encountering novel realizations of either type of bursts that derive from appending another set of fast nullclines to the phase plane. At present, however, we maintain focus on the most common scenarios for the long and short bursts, the details of which are displayed in Fig. 10(a) and (b). The intuition based on the two-neuron case would imply that the long bursts arise by the escape mechanism from the $2g_c$ map and extend approximately to the external crisis of the $1g_c$ map, whereas the short bursts are triggered by the release mechanism and follow the isolated map. The fact that the short bursts contribute decisively to synchronization, while taking place on the isolated map, has direct implications for the prevalence of one functional motif over the others in the regime of burst synchronization, as we discuss below. In case of long bursts, the impact of the synaptic delay is manifested in that their initial segment, which is τ steps long, takes place on the $2g_c$ map. Nonetheless, the whole event becomes less likely once the initial part reaches the external crisis of this map, as it happens for the delays provided by the curve $\tau_{SH}(g_c)$ in Fig. 10(c). Above the values outlined, there are two possible outcomes for the phase point at the external crisis: it either tumbles terminating the burst or the burst may resume so that the phase point traverses from the chaotic attractor of the $2g_c$ map onto that of the $1g_c$ map, describing a heteroclinic trajectory near the latter's saddle fixed point. Either way, the net result is the coexistence of long and short bursts within the time series, which prompts a large fluctuation of the bursts' duration. The presence of the typical long bursts reduces up until $\tau \approx \tau_L(g_c)$, whereby their last sustainable waveform make up the bursts 2τ steps long, whose sections on the $1g_c$ and $2g_c$ maps are approximately equal. One should caution against taking the paradigm so far literally, since alongside the mentioned realizations of long and short bursts being the immediate extrapolation of the two-neuron case, there are other realizations as well, whose number increases with g_c. This is induced by the rise of the metric distance between the saddle-nodes of the $1g_c$ and $2g_c$ maps harboring

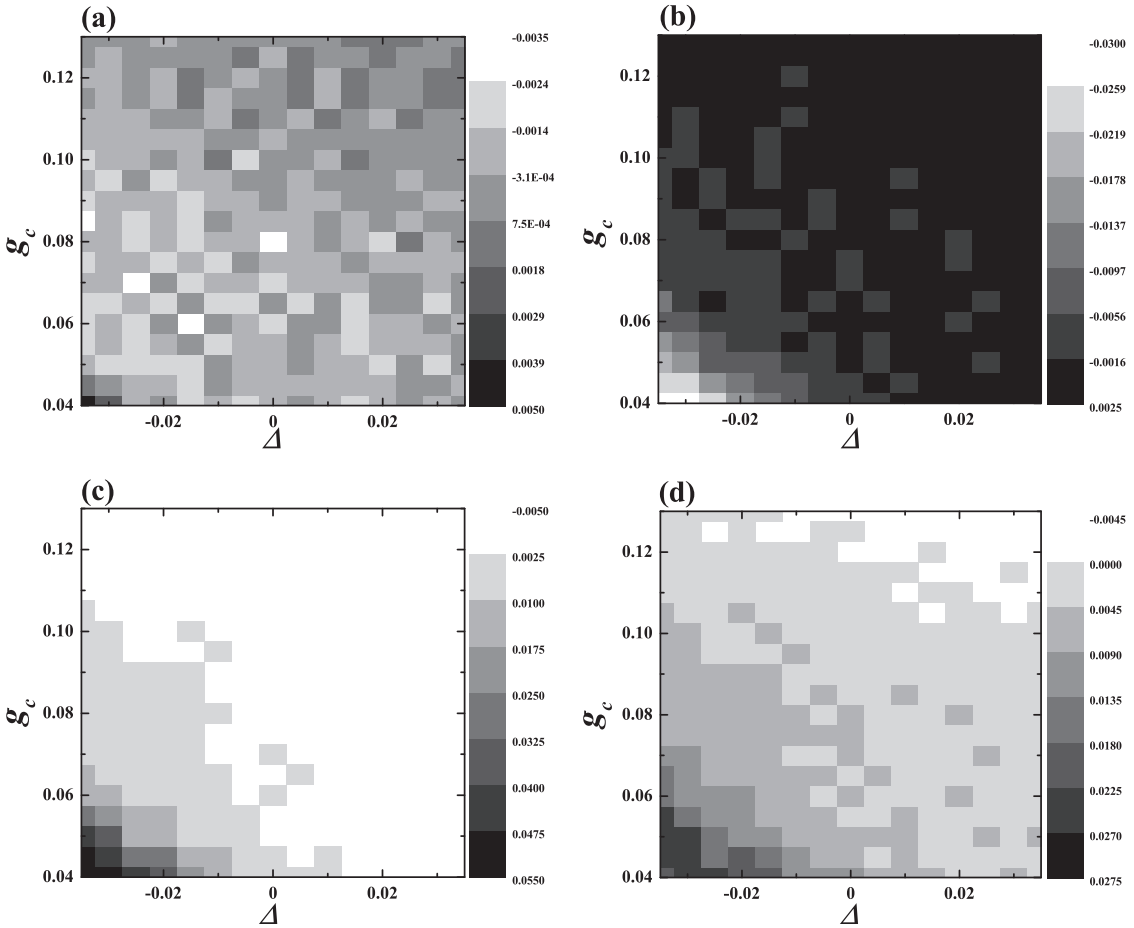

Fig. 11. The effects on fractions of distinct dynamical configurations exerted by the synaptic heterogeneity introduced so as to preserve the original rotational invariance, conveying weights in clockwise direction the value g_c, and those in counterclockwise direction $g_c + \Delta$. (a), (b), (c) and (d) display the difference fields of the c-terms relative to the homogeneous case for the respective *ST*, *DT*, *TC* and *TU* triads obtained at $\tau = 80$. Apart from the relative increase in the *DT* contribution and a comparable reduction in the *TC* one's, the major effect concerns the rise of the *TU*-term for a broad range of parameters.

different types of long, as well as short bursts, both occurring mainly via the release mechanism.

Notwithstanding the arguments above, the physical picture does not seem to get overly obscured. In particular, the shape of the curves in Fig. 10(c), or rather their close correspondence with the profile outlining the areas of increase and maximal *H*-synchronization (Fig. 4) suggests that the principal traits of the ternary system behavior may be viewed as counterparts of those exhibited by the neuron pair. The dynamics of the occurrence of short and long bursts, and especially the prevalence of the former over the latter in the regime of burst synchronization exhibited both by the neuron pair and the triplet, may serve as heuristics to explain the contribution of an arbitrary functional motif relative to another, as well as the abundance of the *TU* motif in particular. In light of this, one is able to find the area of synaptic parameters where the co-action of the chemical synapses manifests so that the neurons are taken into a virtual non-interacting state which coincides with the burst synchronization. In other words, in terms of the phase plane analysis, the genuinely synchronized bursts emerge once the neurons are on the isolated map, which is reflected by the prevalence of the *TU* motif at the sufficiently large τ.

The triplet behavior being reminiscent to that of the neuron pair provides another perspective of the regularity plot in Fig. 9, where, at least for the large delays, it seems justified to carry over the type of explanation put forward in the case of synchronization. However, the nontrivial dependence of R at small and moderate τ calls for a more thorough examination of the role played by the long and short bursts. To do so, we determine the average fraction of short bursts within the time series under variation of g_c and τ irrespective of the bursts' onset mechanism, see Fig. 10(d). Then it is made explicit how the irregularity tongue relates to the flattening of the lower lying curves at larger g_c, where the ratio of the short vs long bursts is approximately 1. Such dependence is due to a stronger impact of the mutual interaction leading to a number of the emergent phenomena and the less typical mechanisms for the occurrence of short bursts.

Given that the main body of the current research concerns a homogeneous motif, a question naturally arises as to whether and how robust are the results so far against introducing heterogeneity in the synaptic parameters. Among a variety of possibilities, a plausible approach consists in preserving the rotational invariance of the circuit by assigning the distinct values to weights in clockwise and counterclockwise directions [39,40]. For such a setup, one arrives at an interesting conclusion regarding the fields of differences of the *c*-terms relative to those obtained for the homogeneous motif, cf. Fig. 11, especially considering the large delays, where the approximate synchronization in-phase is to be expected. While the more superficial results of the inhomogeneity present the increased contribution from the *DT*-triad (Fig. 11(b)) and the comparable reduction in that of the *TC*-triad (Fig. 11(c)), as a main point we single out the substantial rise of the *TU*-term in a broader range of weights (see Fig. 11(d)). Recalling the *TU*'s synchronizing epithet, the latter could indicate, at least for the small disparity of weights, that within the time series of the inhomogeneous motif the synchronized bursts may be more frequent as compared to the initial homogeneous motif.

4. Conclusions

One of the principal reasons to study the neuron triplets lies in the fact that their abundance serves as an indicator of the level of clusterization reached within the network. Focusing on a symmetrical closed triplet, our intention has not only been to build on the current understanding of the relationship between the structural and functional circuits, but also to broaden the field by pointing out how multiple forms of the latter may be used to access the different aspects of the collective neuron dynamics. The framework we propose is based on implementing the properties of the chemical synapses following FTM model together with the features of the Rulkov map, allowing one to characterize the evolution of the representative point in the phase plane in terms of switches between the isolated map and the appropriate interacting maps. The classification of the collective states is approached in two distinct ways, with a common trait that consists in matching the effective network configuration with subgraphs of the original graph, counting in both the connected and the unconnected triads. By one scenario, the system states, cast as dynamical configurations, are distinguished with respect to the number of the active neurons, whereas the second scenario, resting on the functional motifs, concerns the ternary sets of maps occupied by the neurons exhibiting burst synchronization. It comes as no surprise that the presence of the particular triads is model contingent. Here the assumed homogeneity of synaptic thresholds manifests in confining the number of the permitted triads to a subset of 4, coined *ST*, *DT*, *TC* and *TU*. This is a corollary of the correlation between the states of openness of the outward synapses from each node, such that all of them need to be either open or closed at the time.

The fractions of the 4 triads attributed to the dynamical configurations and the functional motifs within the time series are quantified by the *c* and *h* terms, respectively. The fields portraying them in the (g_c,τ) parameter plane indicate the prevailing dependence on the delay. As to the dynamical configurations, one singles out two points: first, that there is an area of small τ and moderate g_c where the system state comes close to a pure one, and second, that increasing τ results in a rise in population of the *TC* and *TU* triads on account of those of *ST* and *DT*. In a similar fashion, the establishment of the approximate synchronization in phase for the large τ is accompanied by the dominance of the *TC* and *TU* factors. Interestingly, the details regarding the role assumed by the distinct triads in the synchronization process may best be understood by comparing whether and how much the *h*-quantities deviate from their *c*-counterparts. This is how we arrive at the conclusion that *TU* may genuinely be regarded a synchronizing triad, reflecting the fact how the proper burst synchronization sets in if the bursts occur such that all three neurons are on the isolated map.

Reflecting on how to define and locate the ternary motifs on larger networks or the possibility of the motifs'

eventual generalization, the two approaches have been applied so far. One is based on decomposing the network to ternary motifs, whereas by the other is assumed a nodal-wise extension to motifs of higher degree that are in a topological sense derived from the classes of the neuron triplets [41]. Recalling that here the coupling is supposed to include only the chemical synapses, which, for their part, are expected to give rise to the phenomenon of cluster synchronization [42], the results provided in this paper may best find their application within the first approach. For example, on the scope of a larger network there could be several burst synchronized clusters mutually shifted in phase, whose location would be determined if one were to recognize the *TU* functional motifs. Considering how the ideas behind the c and h-quantities may be put into a broader context, one recalls the two types of methods applied for functional clustering [43], one of which rests on correlation between the activities of the constituents [1], and the other records the sequences related to the transfer of information within the network [2,3]. As to the former, by way of comparison, the quantity h does not indicate solely on a coordination of neurons at the time, but also relates to their setup from the past. On the second concept, the coarse-graining via the quantities c could be understood as means to trace the preferred paths along which the information is propagated. Another attainable goal may be to devise an algorithm for resolving the smaller networks into structural motifs, with their recognition based on the properties of the dynamical configurations and the functional motifs. This may be interpreted in the context of solving the task of reconstructing the a priori unknown structural network utilizing the section-by-section characterization of the recorded time series of its constituent neurons. We suppose that a putative algorithm could gain on the discriminative potential between the c and h-quantities in different parameter regions, whereas it would probably prove sensitive if the action of the environment were described by the colored, rather than the white noise. At this point, it stands to reason that the next stage of research should concern determining the analogs of c and h-quantities in the case when the motif is subjected to various forms of noise.

Acknowledgment

This research was conducted under project No. 171015, supported by the Serbian Ministry of Education and Science.

References

[1] Honey CJ, Kötter R, Breakspear M, Sporns O. PNAS 2007;104:10240.
[2] Eguíluz VM, Chialvo DR, Cecchi GA, Baliki M, Apkarian AV. Phys. Rev. Lett. 2005;94:018102.
[3] Zhou C, Zemanová L, Zamora G, Hilgetag CC, Kurths J. Phys. Rev. Lett. 2006;97:238103.
[4] Sporns O, Chialvo DR, Kaiser M, Hilgetag CC. Trends Cogn. Sci. 2004;8:418.
[5] Sporns O. Networks of the brain. Cambridge: MIT Press; 2011.
[6] Sporns O, Kotter R. PLoS Biol. 2004;2:e369.
[7] Boccaletti S, Latora V, Moreno Y, Chavez M, Hwang DU. Phys. Rep. 2006;424:175.
[8] Bullmore E, Sporns O. Nat. Rev. Neurosci. 2009;10:186.
[9] Milo R, Shen-Orr S, Itzkovitz S, Kashtan N, Chklovskii D, Alon U. Science 2002;298:824.
[10] Milo R, Itzkovitz S, Kashtan N, Levitt R, Shen-Orr S, Ayzenshtat I, et al. Science 2004;303:1538.
[11] Alon U. Nature 2007;8:450.
[12] Song S, Sjostrom PJ, Reigl M, Nelson S, Chklovskii DB. PLoS Biol. 2005;3:e68.
[13] Li C. Phys. Rev. E 2008;78:037101.
[14] Takahashi YK, Kori H, Masuda N. Phys. Rev. E 2009;79:051904.
[15] Rangan AV. Phys. Rev. Lett. 2009;102:158101.
[16] Rabinovich MI, Varona P, Selverston A, Abarbanel HDI. Rev. Mod. Phys. 2006;78:1213.
[17] Belykh I, de Lange E, Hasler M. Phys. Rev. Lett. 2005;94:188101.
[18] Rossoni E, Chen Y, Ding M, Feng J. Phys. Rev. E 2005;71:061904.
[19] Perc M. Biophys. Chem. 2009;141:175.
[20] Wang Q, Perc M, Duan Z, Chen G. Physica A 2010;389:3299.
[21] Hakken H. Brain dynamics: synchronization and activity patterns in pulse-coupled neural nets with delays and noise. Berlin Heidelberg: Springer; 2007.
[22] Ibarz B, Cao H, Sanjuán MAF. Phys. Rev. E 2008;77:051918.
[23] Ivanchenko MV, Osipov GV, Shalfeev VD, Kurths J. Phys. Rev. Lett. 2004;93:134101.
[24] Rulkov NF. Phys. Rev. Lett. 2001;86:183.
[25] de Vries G. Phys. Rev. E 2001;64:051914.
[26] Franović I, Miljković V. Europhys. Lett. 2010;92:68007.
[27] Franović I, Miljković V. Chaos Soliton. Fract. 2011;44:122.
[28] Innocenti G, Morelli A, Genesio R, Torcini A. Chaos 2007;17:043128.
[29] Franović I, Miljković V. Eur. Phys. J. B 2010;76:613.
[30] Burić N, Todorović K, Vasović N. Phys. Rev. E 2008;78:036211.
[31] Hilborn RC, Erwin RJ. Phys. Rev. E 2005;72:031112.
[32] Rowat PF, Selverston AI. J. Comput. Neurosci. 1997;4:103.
[33] Somers D, Koppel N. Biol. Cybernet. 1993;68:393.
[34] Koppel N, Ermentrout GB. In: Fiedler B, editor. Handbook of dynamical systems. Amsterdam: Elsevier; 2002.
[35] Arbib MA, editor. Handbook of brain theory and neural networks. Cambridge: MIT Press; 2003. p. 47.
[36] Alon U. Molecular cell biology lab. <http://www.weizmann.ac.il/mcb/UriAlon/>.
[37] Pikovsky AS, Kurths J. Phys. Rev. Lett. 1997;78:775.
[38] Guo D, Li C. Phys. Rev. E 2009;79:051921.
[39] Shilnikov A, Gordon R, Belykh I. Chaos 2008;18:037120.
[40] Nowotny T, Huerta R, Rabinovich MI. Chaos 2008;18:037119.
[41] Kashtan N, Itzkovitz S, Milo R, Alon U. Phys. Rev. E 2004;70:031909.
[42] Belykh I, Hasler M. Chaos 2011;21:016106.
[43] Feldt S, Waddell J, Hetrick VL, Berke JD, Zochowski M. Phys. Rev. E 2009;79:056104.